Zeolites Hot Paper

How to cite: *Angew. Chem. Int. Ed.* **2022**, *61*, e202112916
International Edition: doi.org/10.1002/anie.202112916
German Edition: doi.org/10.1002/ange.202112916

Zinc Containing Small-Pore Zeolites for Capture of Low Concentration Carbon Dioxide

*Donglong Fu, Youngkyu Park, and Mark E. Davis**

Abstract: *The capture of low concentration CO_2 presents numerous challenges. Here, we report that zinc containing chabazite (CHA) zeolites can realize high capacity, fast adsorption kinetics, and low desorption energy when capturing ca. 400 ppm CO_2. Control of the state and location of the zinc ions in the CHA cage is critical to the performance. Zn^{2+} loaded onto paired anionic sites in the six-membered rings (6MRs) in the CHA cage are the primary sites to adsorb ca. 0.51 mmol CO_2/g-zeolite with Si/Al = ca. 7, a 17-fold increase compared to the parent H-form. The capacity is increased further to ca. 0.67 mmol CO_2/g-zeolite with Si/Al = ca. 2 due to more paired sites for zinc exchange. Zeolites with double six-membered rings (D6MRs) that orient 6MRs into the cages give enhanced uptakes for CO_2 adsorption with zinc exchange. The results reveal that zinc exchanged CHA and several other small pore, cage containing zeolites merit further investigation for the capture of low concentration CO_2.*

Introduction

Carbon dioxide (CO_2) capture is being investigated as an important approach to limit further increases in CO_2 concentration in the atmosphere.[1] The conventional approaches for capturing high concentration (>10%) CO_2 are being developed for addressing emissions from point sources, such as cement plants, power stations, iron/steel industry installations, and oil refineries. However, point source capture by itself will not be able to reduce atmospheric CO_2 as ca. 50% of the anthropogenic emissions are from mobile sources.[2] Direct air capture (DAC) may be able to aid in mitigating global CO_2 amounts originating from point source and non-point source emissions, and allow for onsite technologies for CO_2 storage or utilization (thereby eliminating the need for storage and transport infrastructure).[2–4] DAC is also promising for capture of leaked CO_2 from carbon capture and storage point sources and/or geologic CO_2 storage sites.[5] DAC requires capture from low concentrations of CO_2, ca. 400 ppm CO_2. In addition to DAC, efficient removal of low concentration CO_2 may be useful for other situations such as air purification in space stations and future human space environments, aircraft, submarine, and office buildings, and in medicine, e.g., anesthesia machines.[6,7] In order to create efficient capture technologies for low concentration CO_2 environments, there is a need for new adsorbents.

Capture of CO_2 requires an effective and economic sorbent that possesses merits such as moderate CO_2-binding affinity, fast sorption kinetics, high capacity, good selectivity against other components in the air, easy regeneration with minimal energy input, long-term stability, and low cost.[8–10] In practice, all adsorbents have trace-offs, as shown in Figure 1. For instance, conventional materials like alkaline- or amine-based sorbents can effectively solve several core issues, and are currently being used by Carbon Engineering and Climeworks for DAC, respectively.[11,12] However, they require either high temperature/energy input for regeneration or have time-dependent oxidation, and they can evaporate toxic volatiles into the atmosphere.[2,10] Other sorbent types, such as porous materials supporting amines,[2,13–15] moisture-swing sorbents,[5,16] zeolites[10,17] and metal-organic frameworks (MOFs)[18–20] have been and are currently being investigated for CO_2 capture. Among these, zeolites and MOFs (Figure 1) are physisorbents that are showing promise for CO_2 capture because they have the potential for fast kinetics and low energy requirements for regeneration that could drastically reduce the cost of operations.[9,10] These properties will likely be particularly significant in applications involving trace CO_2 capture, as the low concentrations of CO_2 often result in both low diffusion rates and low CO_2 capacities.[21] Although it is challenging for these materials to maintain CO_2 capacity under humid conditions, this can be solved by either synthesizing hydrophobic materials[22] or engineering multi-

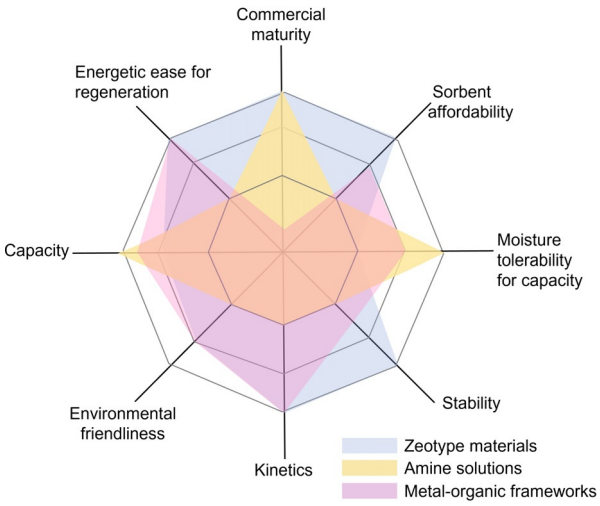

Figure 1. Radar chart illustrating some of the key features that materials need to address for use with CO_2 capture. Radar charts with other criteria are available in Ref. [8].

[*] Dr. D. Fu, Y. Park, Prof. Dr. M. E. Davis
Chemical Engineering, California Institute of Technology
1200 E. California Blvd., Pasadena, CA 91125 (USA)
E-mail: mdavis@cheme.caltech.edu

Supporting information and the ORCID identification number(s) for the author(s) of this article can be found under: https://doi.org/10.1002/anie.202112916.

bed systems with guard desiccant bed before the sorbents.[23,24] Here, we focus on zeolites as they are used in many commercial applications including catalysis, adsorption and separation due to their physical and chemical stabilities.[25–27] They can be synthesized at very large scale over a broad range of properties, e.g., very hydrophilic to very hydrophobic. Zeolites already have shown promising performance for CO_2 capture in post-combustion carbon capture processes as well as CO_2 removal in air pre-purification processes (including the international space station, where a desiccant bed is used prior to the zeolite bed for CO_2 capture).[9,23,28,29]

Although numerous zeolites have been investigated for carbon capture,[30–35] the research for capture of low concentrations of CO_2 (ca. 400 ppm) is scarce, and has mainly been focused on low-silica zeolites of the FAU-type (Si/Al less than 2).[10,17,36] Low-silica zeolites have high H_2O affinity as well as low hydrothermal stability that likely will present challenges for large scale commercialization of carbon capture technologies.[37] Here, we report a successful design of zinc exchanged CHA-type zeolites (Figure 2a) with elevated Si/Al that give higher CO_2 capacity, faster adsorption kinetics, and lower desorption energy for both CO_2 and H_2O than the standard 13X (FAU-type with Si/Al = 1.1), when adsorb CO_2 at 30 °C with a gas mixture of 400 ppm CO_2/400 ppm Ar (internal standard)/ He. SSZ-13 zeolites (synthetic CHA-type) were prepared, as they can be synthesized over a very broad range of Si/Al and are commercially available at several Si/Al.[38,39] Also, SSZ-13 has demonstrated promising CO_2 adsorption performance and CO_2/N_2 selectivity for capturing high concentration CO_2.[40–48] We demonstrate here that the choice of the zeolite as well as the state and location of zinc ions are crucial for the CO_2 adsorption performance. We denote zinc as Zn throughout, but want to make it clear that this notation does not imply zinc metal. All zinc analyzed in this study is in the form of a cation (there are several types).

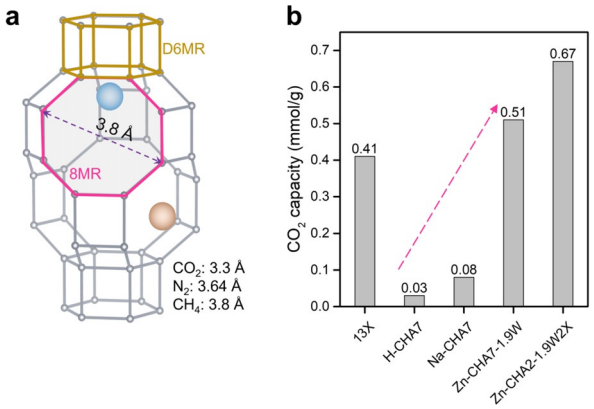

Figure 2. Performance of zinc ion exchanged CHA-type zeolites for CO_2 adsorption. a) CHA cage with 8-membered ring (8MR) and double 6-membered ring (D6MR) highlighted in pink and gold, respectively. Extra-framework cation locations are shown by brown and blue spheres in the 8MR and below the D6MR, respectively. b) The capacities for CO_2 adsorption in ion-exchanged CHA-type (M-CHAR-NW2X) zeolites, where M, R and N indicate the extra-framework cation type, Si/Al ratio and ion concentrations of aqueous solutions, respectively. If W is not included, the material was not washed with distilled H_2O after ion exchange, and if no value is listed after W, then only one exchange was performed. Zeolite 13X is used for comparison since it is a standard and top-performing zeolite adsorbent for direct air capture (DAC).

Results and Discussion

CHA-type zeolites possess the CHA framework topology (Figure 2a) that consists of CHA cages connected via double six-membered rings (D6MRs), and have small pores (those that are constructed from 8 T-atoms (Si + Al) and 8 oxygen atoms -denoted as 8-membered ring, 8MRs).[49] Here, CHA-type materials were synthesized with different Si/Al ratios (see physicochemical properties in Figures S1–S5 and Table S1). The samples were denoted as M-CHAR-NW, where M, R and N indicate the extra-framework cation type, Si/Al ratio, ion concentrations of aqueous solutions and samples washed with a copious amount of H_2O after ion exchange, respectively. If W is not included, the material was not washed with distilled H_2O after ion exchange, and if no value is listed after W, then only one exchange was performed. Column breakthrough experiments (see details in Figure S6) in a fixed-bed were used to examine the CO_2 capture performance, as this method provides breakthrough capacity, saturation capacity and diffusion kinetics, as well as desorption energy when coupled with temperature programmed desorption (TPD).

Alkali-ion containing SSZ-13 zeolites have been shown to adsorb CO_2 due to the strong electric field and acid-base interaction induced by the ions.[32,44] Our results (Figure 2b) show that Na-CHA7-0.5 gives a two-fold increase of CO_2 capacity over the H-CHA7 zeolite. In order to test the effect of the varying number of ions in the solids on adsorption capacity, Na-CHA zeolites with different Si/Al ratios were investigated. The adsorption capacity (Table S2) for the zeolites with Si/Al ratios of 2, 5, 7, 9 and 20 are all substantially lower (0.16 mmol g^{-1} or less) than that of the 13X zeolite (0.41 mmol g^{-1}). Note that 13X zeolite has reported values in the literature of 0.40–0.41 mmol g^{-1} for CO_2 concentrations between 395–500 ppm, validating the reliability of our method.[7,17,36]

As it was not possible to obtain high CO_2 capacity using Na-CHA zeolites, alternative cation types were investigated for CO_2 adsorption in CHA-type zeolites. Several ions exchanged into CHA-type zeolites exhibited increased CO_2 adsorption capacities as shown in Figure S7 and Table S2. Specifically, Zn, Nickel (Ni) and Indium (In) ions exchanged into H-CHA7 show CO_2 capacities of 0.17, 0.14 and 0.08 mmol g^{-1}, respectively. The CO_2 capacity of Zn-CHA7-0.5 (Figure S8) is increased to 0.28 mmol g^{-1} by simply washing the materials after ion-exchanged (denoted as Zn-CHA7-0.5W). An increased CO_2 capacity of ca. 0.51 mmol g^{-1} (Figure 2b) was resulted for Zn-CHA7-1.9W, and the value is larger than that obtained from 13X zeolites. The CO_2 capacities are a function of the Si/Al ratios of the CHA-type zeolites (Figure S9), as more Zn ions can be exchanged into lower Si/Al frameworks. Successful synthesis of CHA-type zeolite with Si/Al = 2 (details in Supporting Information) and then ion exchanged to give Zn-CHA2-1.9W2X shows the highest CO_2 capacity of ca. 0.67 mmol g^{-1} (Figure 2b). This

substantial increase in adsorption capacity maybe useful for applications that involve multi-bed system with dried inputs to the CO_2 capture adsorbents (as described above). Zn-CHA zeolites have been reported for CO_2 adsorption at higher pressure.[43,48] However, a lower adsorption capacity was observed for Zn-CHA compared to its H-form counterpart.[43] This seemingly contrary result to the data obtained here at low concentration of CO_2 could be due to differences in the preparation of Zn containing zeolites. In order to better understand the structural features that provide the high adsorption capacity observed in this work, the active sites for CO_2 adsorption were investigated and discussed below.

The Zn-CHA-type materials exhibit faster adsorption kinetics than 13X, as illustrated by the sharper breakthrough profile for Zn-CHA7-1.9W compared to 13X (Figure 3a). This results in a smaller difference between breakthrough and saturation capacities. Similar results were observed for all Zn-CHA zeolites (physicochemical properties in Table S3) studied in this work (Figures S10–S11). Furthermore, a lower desorption energy of CO_2 was observed for Zn-CHA7-1.9W than 13X (Figure S12 and Table S4). Fourier-transform infrared (FTIR, Figure S13) spectra reveal that CO_2 molecules are exclusively physisorbed in Zn-CHA zeolites. However, besides physisorbed CO_2 molecules, chemisorbed, carbonate-like species are observed in 13X zeolite.[17,50] Indeed, multicycle experiments (Figure S14) suggest that Zn-CHA zeolites show high recyclability (>80%) at temperatures as low as 60 °C under ambient pressure, while low recyclability is reported in 13X when the temperature is lower than 261 °C due to its high affinity to CO_2.[17] Moreover, TGA results (Figure S15) show that the Zn-CHA7 zeolite adsorbs less H_2O (12.51 wt%) than 13X (19.78 wt%) after equilibrating under the same humid environments (ca. 20% relative humidity), suggesting the former possesses higher hydrophobicity. Zn-CHA zeolite also gives promising performance for 400 ppm CO_2 adsorption under a gas stream with 49% relative humidity. Specifically, Zn-CHA7-1.9W exhibits 1.5 times breakthrough CO_2 capacity (0.22 mmol g^{-1}) of that for 13X (0.15 mmol g^{-1}), while their saturation capacities are comparable (0.22 mmol g^{-1}). Due to the weaker affinity to CO_2 (Figures S12–S13) and H_2O (Figure S15), Zn-CHA7-1.9W shows lower desorption temperature maxima (Figure 3b) for both CO_2 and H_2O than 13X, indicating the potential of utilizing the former in a single bed adsorption system for certain circumstances. We are currently exploring further the competitive behavior of CO_2 and H_2O with the Zn-CHA materials as there are many different adsorption and desorption situations that may be applicable to commercial application.

Table 1: Chemical compositions and CO_2 capacities of the H-form CHA zeolites as well as the representative Zn-CHA7 and Zn-CHA(K)7 samples.

Samples	Zn/Al[b]	SiAlOH [mmol g^{-1}][c]	Zn^{2+}/ U.C.[d]	$Zn(OH)^+$/ U.C.[d]	CO_2/ U.C.
H-CHA7	0.00	1.26	0.00	0	0.06
Zn-CHA7-0.002W[a]	0.08	1.10	0.21	0.12	0.27
Zn-CHA7-0.015W[a]	0.23	0.82	0.54	0.44	0.55
Zn-CHA7-0.02W[a]	0.29	0.73	0.54	0.67	0.60
Zn-CHA7-1.9W	0.54	0.33	0.96	1.64	1.21
Zn-CHA7-0.5W	0.87	0.11	0.36	3.56	0.69
H-CHA(K)7	0	1.25	0	0	–
Zn-CHA(K)7-1.9W2X	0.31	0.55	1.19	0.28	0.64

[a] Ion exchange experiments were performed in Zn^{2+} aqueous solution with pH adjusted to 4.92 by adding 0.1 M HCl aqueous solution. If not labeled, pH was uncontrolled for those materials during ion exchanges. [b] Elemental analysis was performed using EDS. [c] Concentration of Brønsted acidic protons (SiOHAl) calculated from the ^{1}H MAS NMR spectra. [d] Zn^{2+} or $Zn(OH)^+$ ions per unit cell SSZ-13 calculated from the EDS results and SiOHAl density. More information can be found in Tables S6 and S8 in Supporting Information.

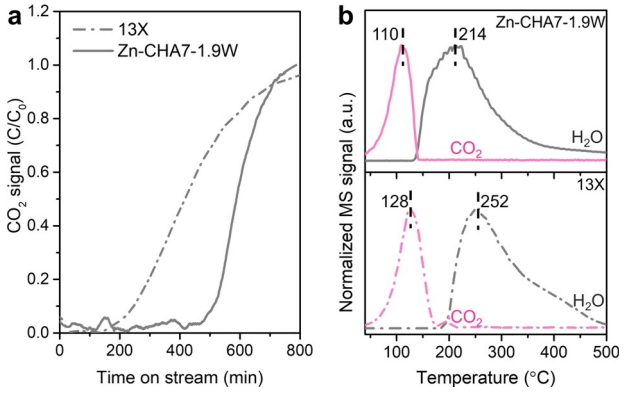

Figure 3. Comparison of gas sorption behavior of 13X and Zn-CHA zeolites. a) Column breakthrough profiles of 13X and Zn-CHA7-1.9W zeolites for the adsorption of dry CO_2. b) Temperature programmed desorption profiles of CO_2 and H_2O from Zn-CHA7-1.9W and 13X zeolites after saturation with humid CO_2 (relative humidity = 49%). The composition of the CO_2 gas for adsorption under both dry and humid conditions is ca. 400 ppm CO_2/400 ppm Ar (internal standard)/He. Desorption experiments were performed with a ramp rate of 10 °C min^{-1} to 500 °C under a 5% Ar/He gas stream.

To dissect the active sites for low concentration CO_2 adsorption, a series of Zn-CHA7 samples were prepared with fixed Al composition (Si/Al = 7) and Zn/U.C. ranging from 0 to 6.60 (Table 1 and S5), where Zn/U.C. denotes the number of Zn ions per CHA unit cell, i.e., Zn ion density. As shown by the data in Figure 4a, a volcano shape profile with three distinct stages was observed. CO_2 capacity increases at two different rates (stage I and stage II) before declining when the Zn ion loading is higher than ca. 2.60 Zn/U.C. Simultaneously, the adsorption efficiency, i.e., CO_2 per Zn ion, gradually decreases with the increase of Zn ion loading. Nitrogen physisorption results show that the micropore volume of parent CHA7 is 0.24 $cm^3 g^{-1}$, being consistent with previously reported values of SSZ-13.[35] The micropore volumes declines upon loading of Zn ions, and comparable micropore volumes (0.18–0.21 $cm^3 g^{-1}$, Table S3) are obtained for Zn-CHA7 with Zn ion density lower than 6.60/U.C. Thus, the distinct behaviors at the three stages, as well as the variations of CO_2 capacities, are due to the speciation of Zn ions. The environments and states of Zn ions were examined to understand the CO_2 adsorption behavior. As shown in Figure 4b, two new FTIR features are seen at ca. 902 and

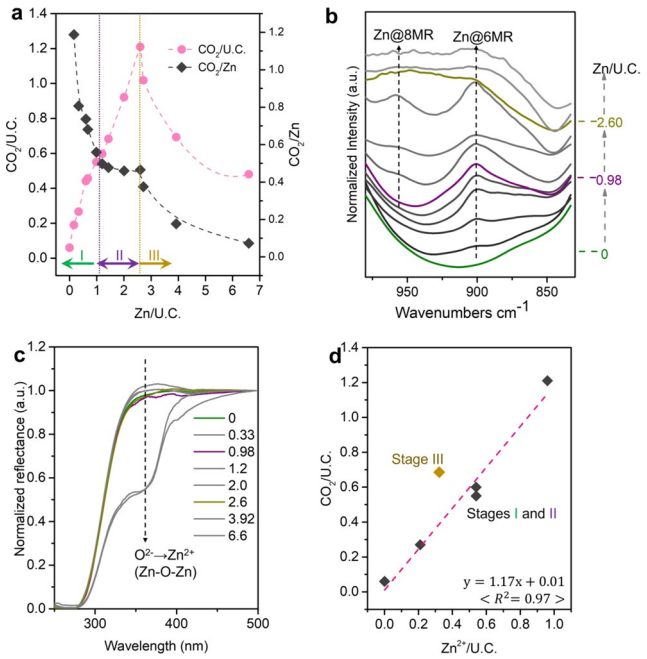

Figure 4. Speciation of Zn ions in the CHA-type zeolites and the impact on CO_2 adsorption. a) CO_2 capacity per unit cell (CO_2/U.C.) of Zn-CHA7 samples with increasing Zn ion density (Zn/U.C.). Adsorption was performed at 30 °C with a gas mixture of 400 ppm CO_2/400 ppm Ar (internal standard)/He. b) The FT-IR spectra for the framework T-O-T vibration of Zn-CHA7 materials with various Zn ion loading. c) UV/Vis diffuse reflectance spectra of Zn-CHA7 zeolites with various Zn ion loading. d) Correlation of the number of Zn^{2+} and CO_2 per unit cell. Dashed lines are interpolations to guide the eye.

950 cm^{-1} for the Zn-CHA7 samples in comparison to H-CHA7 (Zn/U.C. = 0). These vibrations are assigned to perturbed T-O-T structural vibrations in the vicinity of extra-framework cations occupying sites in the 6MRs and 8MRs in the CHA cage, respectively.[51–53] The observed locations of Zn ions are consistent with the results from the recent single crystal X-ray structural analysis of Zn ion exchanged large natural CHA, which demonstrates Zn ions sit in the 6MRs (outside of the D6MRs) and the CHA cage (near the 8MRs).[54] Notably, only one band at 902 cm^{-1} appears for Zn-CHA samples at stage I followed by the evolution of an extra band at 950 cm^{-1} at stage II (Zn/U.C. > 1.21). These results suggest that the Zn ions are exclusively located in the 6MRs at stage I, and that further increase of the Zn ion loading results in the addition of Zn ions to the 8MRs. The UV/Vis diffuse reflectance (Figure 4c) results show the formation of Zn-O-Zn species solely at stage III with high Zn ion loadings,[55,56] as suggested by the appearance of the $O^{2-} \rightarrow Zn^{2+}$ ligand-to-metal charge transfer transition band at ca. 360 nm.[57] Thus, Zn ions are incorporated as Zn^{2+} and/or $Zn(OH)^+$ ions (Figures S16–21, with detailed discussion in Supporting Information) at stages I and II, consistent with previous research on copper ion exchange into CHA-type zeolites.[58]

Quantitative analysis of the state of Zn ions (Tables 1 and S6) suggests that Zn^{2+} ions are the predominant species at stage I (Zn/Al ≤ 0.23) that shows high adsorption efficiency, i.e., CO_2/Zn. Correlation of the numbers of Zn^{2+} and CO_2/U.C. gives a linear relation (Figure 4d) at stages I and II. These results are consistent with Zn^{2+} being the primary adsorption site. Divalent ions (M^{2+}) are known to balance the paired anionic sites introduced by the paired aluminum (2Al) sites in zeolites. Previous studies show that the 2Al sites are preferentially located in the 6MRs in the CHA cage, for SSZ-13 zeolites that are synthesized using methods similar to this work with Na^+ as the inorganic mineralizer.[59,60] Co^{2+} titration of the density of the 2Al sites in 6MR (Table S7) shows a Co^{2+}/Al of 0.20 ± 0.02 for the CHA7 zeolites, fitting the predicted value from the literature.[59] Importantly, the highest value of Zn^{2+}/Al obtained in the CHA7 is ca. 0.20, which is in good agreement with the Co^{2+}/Al. Therefore, we put forth the model where (see detailed discussion in Supporting Information) the Zn^{2+} ions responsible for the adsorption of CO_2 are located in the 6MRs in the CHA cage (as observed from the single crystal X-ray structural solution[54]). Additionally, Zn-O-Zn is likely an extra site for CO_2 adsorption, as it is the only new species appearing at stage III with CO_2/U.C. vs. Zn^{2+}/U.C. sitting above (Figure 4d) the linear correlation.

To assess if Zn^{2+} ions in the 6MRs are significant for CO_2 adsorption, further study was performed using K^+ directed SSZ-13 zeolites (Si/Al = ca. 7, denoted as CHA(K)7) with 2Al dominated in the 8MRs (Figures S22–S28 and Table S8, with detailed discussion in Supporting Information).[60] ^{1}H NMR results (Table 1) show comparable proton densities for the proton form of CHA(K)7 (1.25 mmol g^{-1}) and CHA7 (1.26 mmol g^{-1}). Analysis of the residual H^+ density (Figure S24) of the Zn-CHA(K)7 zeolites indicates that each Zn ion consumes two H^+ in the 8MRs and one H^+ in the 6MRs. In contrast, close to one H^+ is replaced by each Zn ion in the 8MRs of the Zn-CHA7 counterpart (Figure S19), and the value is two for Zn ion loaded to the 6MRs. These results suggest that Zn-CHA(K)7 zeolites contain Zn^{2+} primarily in the 8MRs, which allows a side-by-side comparison with the Zn-CHA7 materials with Zn^{2+} ions in the 6MRs to examine the significance of the location of Zn^{2+} for CO_2 adsorption. Surprisingly, the adsorption results show that CO_2 capacity remained almost constant when loading Zn^{2+} ions in the 8MRs (Figures S26). Quantification analysis (Table 1 and S27) shows that locating Zn^{2+} ions in the 8MRs with 1.19 Zn^{2+}/U.C. only adsorbs 0.64 CO_2/U.C. This is markedly lower than the 1.21 CO_2/U.C. obtained for Zn-CHA zeolites with 0.96 Zn^{2+}/U.C. in the 6MRs (Table 1). An adsorption efficiency of 0.65 CO_2/Zn (Table S8) was observed for Zn-CHA(K)7 with $Zn(OH)^+$ dominated in the 6MRs, suggesting that a limited fraction of $Zn(OH)^+$ species located in the 6MRs are able to adsorb CO_2. This could be attributed to the heterogeneous nature of the Al sites in CHA cages, leading to different environments/energies for the same extra-framework species.[27] However, all of the Zn^{2+} in the 6MRs could adsorb CO_2 with an efficiency of 1.17 CO_2/Zn^{2+} (Figure 4d). This result would lead to the conclusion that the Zn^{2+} ions in the 8MRs are likely inactive or less effective than those located at the 6MRs, and thus highlighting the significance of locating Zn^{2+} species in the 6MRs for high CO_2 adsorption capacity. Collectively, these results show that Zn^{2+} ions in the 6MRs are the primary sites for CO_2 adsorption. This explains the observed positive correlation (Figure 2b) between CO_2

capacity and Al content in the Zn-CHA7 and Zn-CHA2 zeolites, as the latter have more 2Al (Table S1 and Figure S5) in the 6MRs that can accommodate more Zn^{2+}.[59] In contrast, Zn-CHA5 (Table S2) adsorbs less CO_2 than Zn-CHA7 due to the lower number of 2Al in CHA5 (Table S1 and Figure S5). Therefore, the Al distribution in the framework with maximizing Al located in 6MRs as 2Al sites has a critical effect on the enhanced CO_2 adsorption performance.

In order to assist in verifying the significance of 2Al sites as well as their locations in zeolites for accommodating Zn^{2+} ions for CO_2 adsorption, two groups of zeolites were selected (Figure 5). Group I (Figure S29) is small-pore zeolites with framework topologies more like the CHA-type. Group II (Figure S30) includes the standard low-silica zeolite adsorbents, namely FAU-type (13X) and LTA-type (zeolite A). As shown in Figure 5, Zn ion exchange in zeolites from group I (AEI, AFX) shows increased capacities for CO_2 adsorption. This is attributed to the presence of abundant 6MRs in these frameworks that can preferentially accommodate the divalent ions (Zn^{2+}), as shown in previous studies of copper ion exchanged AEI[61] and AFX.[62] For group II, the addition of Zn ions surprisingly prohibits the adsorption of CO_2 in these zeolites. These results are consistent with those from higher pressure (> 0.66 mbar) adsorption where CO_2 capacity decreased with the addition of Zn ions into 13X.[30] The significant decline in CO_2 adsorption is corroborated by the negligible absorption in the CO_2 vibration region as shown in the FTIR spectra (Figures S31 and S32). This observation could be attributed to the preferential location of divalent ions inside sodalite (SOD) cages or in the center of the hexagonal prism D6MRs in these materials (Figure S30 with detailed discussion) that are inaccessible to CO_2 molecules.[30,63] These results altogether indicate that the framework topology and thus the positioning of extra-framework cations dictate their CO_2 adsorption properties. Specifically, the lack of SOD cages and the abundance of accessible 6MRs are two crucial factors for CO_2 adsorption in the Zn ion exchanged zeolites.

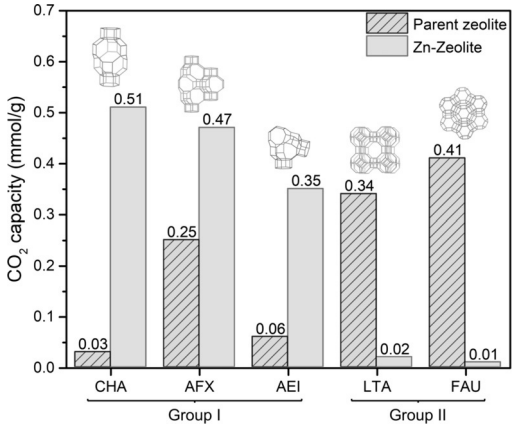

Figure 5. Zeolite topology-dependent CO_2 adsorption. Groups I is small-pore zeolites with framework topologies more like the CHA-type. Group II includes the standard low-silica zeolite adsorbents. Adsorption experiments were performed at 30 °C with a gas mixture of 400 ppm CO_2/400 ppm Ar (internal standard)/He.

Conclusion

The addition of Zn cations into CHA-type zeolites, e.g., SSZ-13, produced greatly enhanced performance for adsorbing low concentrations of CO_2. The Zn ion containing zeolites exhibited higher CO_2 capacity, faster kinetics, lower desorption energy than the standard low-silica 13X zeolites. Control of the state and location of Zn ions in the CHA cages was crucial to the high CO_2 adsorption capacity. Zn^{2+} ions located at the 6MRs of SSZ-13 with Si/Al = ca. 7 gave an adsorption capacity of 0.51 mmol CO_2/g-zeolite, a 17-fold increase compared to the parent H-form. Lowering the Si/Al to ca. 2 resulted in an increase of capacity to 0.67 mmol CO_2/g-zeolite. Investigating zeolites with different topologies further highlights that the position of divalent ions plays a significant role in the enhancement of the capacity for CO_2 adsorption. The results presented here suggest that Zn ions exchanged CHA and several other small-pore zeolites are interesting physisorbents that merit further investigation for the capture of CO_2 from low concentration environments that may include DAC.

Acknowledgements

This work was financially supported by Carbon Capture, Inc. Y.P. would like to thank Kwanjeong Eduional Foundation for the financial support. The authors acknowledge Dr. Stacey I. Zones (Chevron) for providing chemicals for the synthesis of the AFX-type zeolite. Faisal Alshafei (California Institute of Technology) is thanked for synthesizing the OSDA for the synthesis of the AEI-type zeolite.

Conflict of Interest

A US patent (application No. 63154334) related to this work has been applied by D. Fu and M. E. Davis as co-inventors. M. E. Davis is a consultant for Carbon Capture, Inc.

Keywords: adsorption · carbon capture · physisorbents · small-pore zeolites · zinc

[1] K. S. Lackner, S. Brennan, J. M. Matter, A.-H. A. Park, A. Wright, B. van der Zwaan, *Proc. Natl. Acad. Sci. USA* **2012**, *109*, 13156 – 13162.
[2] E. S. Sanz-Pérez, C. R. Murdock, S. A. Didas, C. W. Jones, *Chem. Rev.* **2016**, *116*, 11840 – 11876.
[3] C. Brady, M. E. Davis, B. Xu, *Proc. Natl. Acad. Sci. USA* **2019**, *116*, 25001 – 25007.
[4] C. Breyer, M. Fasihi, C. Bajamundi, F. Creutzig, *Joule* **2019**, *3*, 2053 – 2057.
[5] X. Shi, H. Xiao, H. Azarabadi, J. Song, X. Wu, X. Chen, K. S. Lackner, *Angew. Chem. Int. Ed.* **2020**, *59*, 6984 – 7006; *Angew. Chem.* **2020**, *132*, 7048 – 7072.
[6] O. Shekhah, Y. Belmabkhout, Z. Chen, V. Guillerm, A. Cairns, K. Adil, M. Eddaoudi, *Nat. Commun.* **2014**, *5*, 4228.
[7] S. Mukherjee, N. Sikdar, D. O'Nolan, D. M. Franz, V. Gascón, A. Kumar, N. Kumar, H. S. Scott, D. G. Madden, P. E. Kruger, B. Space, M. J. Zaworotko, *Sci. Adv.* **2019**, *5*, eaax9171.

[8] R. L. Siegelman, E. J. Kim, J. R. Long, *Nat. Mater.* **2021**, *20*, 1060 – 1072.
[9] S. Choi, J. H. Drese, C. W. Jones, *ChemSusChem* **2009**, *2*, 796 – 854.
[10] A. Kumar, D. G. Madden, M. Lusi, K.-J. Chen, E. A. Daniels, T. Curtin, J. J. Perry, M. J. Zaworotko, *Angew. Chem. Int. Ed.* **2015**, *54*, 14372 – 14377; *Angew. Chem.* **2015**, *127*, 14580 – 14585.
[11] H. Azarabadi, K. S. Lackner, *Appl. Energy* **2019**, *250*, 959 – 975.
[12] M. Fasihi, O. Efimova, C. Breyer, *J. Cleaner Prod.* **2019**, *224*, 957 – 980.
[13] S. A. Didas, S. Choi, W. Chaikittisilp, C. W. Jones, *Acc. Chem. Res.* **2015**, *48*, 2680 – 2687.
[14] J. J. Lee, C.-J. Yoo, C.-H. Chen, S. E. Hayes, C. Sievers, C. W. Jones, *Langmuir* **2018**, *34*, 12279 – 12292.
[15] A. R. Sujan, S. H. Pang, G. Zhu, C. W. Jones, R. P. Lively, *ACS Sustainable Chem. Eng.* **2019**, *7*, 5264 – 5273.
[16] M. Oschatz, M. Antonietti, *Energy Environ. Sci.* **2018**, *11*, 57 – 70.
[17] S. M. W. Wilson, F. H. Tezel, *Ind. Eng. Chem. Res.* **2020**, *59*, 8783 – 8794.
[18] P. M. Bhatt, Y. Belmabkhout, A. Cadiau, K. Adil, O. Shekhah, A. Shkurenko, L. J. Barbour, M. Eddaoudi, *J. Am. Chem. Soc.* **2016**, *138*, 9301 – 9307.
[19] K. Sumida, D. L. Rogow, J. A. Mason, T. M. McDonald, E. D. Bloch, Z. R. Herm, T.-H. Bae, J. R. Long, *Chem. Rev.* **2012**, *112*, 724 – 781.
[20] D. M. D'Alessandro, B. Smit, J. R. Long, *Angew. Chem. Int. Ed.* **2010**, *49*, 6058 – 6082; *Angew. Chem.* **2010**, *122*, 6194 – 6219.
[21] J. Liu, Y. Wei, Y. Zhao, *ACS Sustainable Chem. Eng.* **2019**, *7*, 82 – 93.
[22] M. Ding, R. W. Flaig, H.-L. Jiang, O. M. Yaghi, *Chem. Soc. Rev.* **2019**, *48*, 2783 – 2828.
[23] R. Kay, *SAE Trans.* **1998**, *107*, 514 – 522.
[24] G. E. Cmarik, J. C. Knox, CO_2 Removal for the International Space Station—4-Bed Molecular Sieve Material Selection and System Design, 49th International Conference on Environmental Systems, Massachusetts, Boston, **2019**.
[25] E. M. Flanigen, R. W. Broach, S. T. Wilson, in *Zeolites in Industrial Separation and Catalysis* (Ed.: S. Kulprathipanja), Wiley-VCH, Weinheim, **2010**, pp. 1 – 26.
[26] Y. Li, L. Li, J. Yu, *Chem* **2017**, *3*, 928 – 949.
[27] M. E. Davis, *Nature* **2002**, *417*, 813 – 821.
[28] K. T. Chue, J. N. Kim, Y. J. Yoo, S. H. Cho, R. T. Yang, *Ind. Eng. Chem. Res.* **1995**, *34*, 591 – 598.
[29] S. Sircar, W. C. Kratz, *Removal of Water and Carbon Dioxide from Air*, US4249915A, **1981**.
[30] A. Khelifa, Z. Derriche, A. Bengueddach, *Microporous Mesoporous Mater.* **1999**, *32*, 199 – 209.
[31] V. P. Shiralkar, S. B. Kulkarni, *Zeolites* **1985**, *5*, 37 – 41.
[32] K. S. Walton, M. B. Abney, M. Douglas LeVan, *Microporous Mesoporous Mater.* **2006**, *91*, 78 – 84.
[33] T.-H. Bae, M. R. Hudson, J. A. Mason, W. L. Queen, J. J. Dutton, K. Sumida, K. J. Micklash, S. S. Kaye, C. M. Brown, J. R. Long, *Energy Environ. Sci.* **2013**, *6*, 128 – 138.
[34] Y. Zhou, J. Zhang, L. Wang, X. Cui, X. Liu, S. S. Wong, H. An, N. Yan, J. Xie, C. Yu, P. Zhang, Y. Du, S. Xi, L. Zheng, X. Cao, Y. Wu, Y. Wang, C. Wang, H. Wen, L. Chen, H. Xing, J. Wang, *Science* **2021**, *373*, 315 – 320.
[35] J. A. Thompson, S. I. Zones, *Ind. Eng. Chem. Res.* **2020**, *59*, 18151 – 18159.
[36] N. R. Stuckert, R. T. Yang, *Environ. Sci. Technol.* **2011**, *45*, 10257 – 10264.
[37] N. S. Wilkins, J. A. Sawada, A. Rajendran, *Adsorption* **2020**, *26*, 765 – 779.
[38] J. H. Kwak, R. G. Tonkyn, D. H. Kim, J. Szanyi, C. H. F. Peden, *J. Catal.* **2010**, *275*, 187 – 190.
[39] I. Bull, W.-M. Xue, P. Burk, R. S. Boorse, W. M. Jaglowski, G. S. Koermer, A. Moini, J. A. Patchett, J. C. Dettling, M. T. Caudle, *Copper CHA Zeolite Catalysts*, US7601662B2, **2009**.
[40] T. D. Pham, Q. Liu, R. F. Lobo, *Langmuir* **2013**, *29*, 832 – 839.
[41] M. R. Hudson, W. L. Queen, J. A. Mason, D. W. Fickel, R. F. Lobo, C. M. Brown, *J. Am. Chem. Soc.* **2012**, *134*, 1970 – 1973.
[42] J. Shang, G. Li, R. Singh, Q. Gu, K. M. Nairn, T. J. Bastow, N. Medhekar, C. M. Doherty, A. J. Hill, J. Z. Liu, P. A. Webley, *J. Am. Chem. Soc.* **2012**, *134*, 19246 – 19253.
[43] M. Sun, Q. Gu, A. Hanif, T. Wang, J. Shang, *Chem. Eng. J.* **2019**, *370*, 1450 – 1458.
[44] J. Zhang, R. Singh, P. A. Webley, *Microporous Mesoporous Mater.* **2008**, *111*, 478 – 487.
[45] M. Debost, P. B. Klar, N. Barrier, E. B. Clatworthy, J. Grand, F. Lainé, P. Brazda, L. Palatinus, N. Nesterenko, P. Boullay, S. Mintova, *Angew. Chem. Int. Ed.* **2020**, *59*, 23491 – 23495; *Angew. Chem.* **2020**, *132*, 23697 – 23701.
[46] J. K. Bower, D. Barpaga, S. Prodinger, R. Krishna, H. T. Schaef, B. P. McGrail, M. A. Derewinski, R. K. Motkuri, *ACS Appl. Mater. Interfaces* **2018**, *10*, 14287 – 14291.
[47] H. J. Kwon, S. C. Kwon, H. C. Lee, W. S. Ahn, S. H. Hong, *Carbon Dioxide Adsorbent Including Zeolite and Methods for Preparing the Same*, US9358530B2, **2016**.
[48] T. Du, *Res. Chem. Intermed.* **2017**, *43*, 1783 – 1792.
[49] M. Dusselier, M. E. Davis, *Chem. Rev.* **2018**, *118*, 5265 – 5329.
[50] T. Montanari, G. Busca, *Vib. Spectrosc.* **2008**, *46*, 45 – 51.
[51] J. Hun Kwak, H. Zhu, J. H. Lee, C. H. F. Peden, J. Szanyi, *Chem. Commun.* **2012**, *48*, 4758 – 4760.
[52] K. Mlekodaj, J. Dedecek, V. Pashkova, E. Tabor, P. Klein, M. Urbanova, R. Karcz, P. Sazama, S. R. Whittleton, H. M. Thomas, A. V. Fishchuk, S. Sklenak, *J. Phys. Chem. C* **2019**, *123*, 7968 – 7987.
[53] Y. Shan, W. Shan, X. Shi, J. Du, Y. Yu, H. He, *Appl. Catal. B* **2020**, *264*, 118511 – 118520.
[54] L. T. Dimowa, I. Piroeva, S. Atanasova-Vladimirova, R. Rusew, B. L. Shivachev, *Bulg. Chem. Commun.* **2018**, *50*, 114 – 122.
[55] J. A. Biscardi, G. D. Meitzner, E. Iglesia, *J. Catal.* **1998**, *179*, 192 – 202.
[56] A. Mehdad, R. F. Lobo, *Catal. Sci. Technol.* **2017**, *7*, 3562 – 3572.
[57] N. Koike, K. Iyoki, S. H. Keoh, W. Chaikittisilp, T. Okubo, *Chem. Eur. J.* **2018**, *24*, 808 – 812.
[58] E. Borfecchia, K. A. Lomachenko, F. Giordanino, H. Falsig, P. Beato, A. V. Soldatov, S. Bordiga, C. Lamberti, *Chem. Sci.* **2015**, *6*, 548 – 563.
[59] C. Paolucci, A. A. Parekh, I. Khurana, J. R. Di Iorio, H. Li, J. D. Albarracin Caballero, A. J. Shih, T. Anggara, W. N. Delgass, J. T. Miller, F. H. Ribeiro, R. Gounder, W. F. Schneider, *J. Am. Chem. Soc.* **2016**, *138*, 6028 – 6048.
[60] J. R. Di Iorio, S. Li, C. B. Jones, C. T. Nimlos, Y. Wang, E. Kunkes, V. Vattipalli, S. Prasad, A. Moini, W. F. Schneider, R. Gounder, *J. Am. Chem. Soc.* **2020**, *142*, 4807 – 4819.
[61] G. Fu, R. Yang, Y. Liang, X. Yi, R. Li, N. Yan, A. Zheng, L. Yu, X. Yang, J. Jiang, *Microporous Mesoporous Mater.* **2021**, *320*, 111060 – 111072.
[62] D. W. Fickel, R. F. Lobo, *J. Phys. Chem. C* **2010**, *114*, 1633 – 1640.
[63] W. P. J. H. Jacobs, J. H. M. C. van Wolput, R. A. van Santen, *Zeolites* **1993**, *13*, 170 – 182.

Manuscript received: September 22, 2021
Accepted manuscript online: November 19, 2021
Version of record online: December 18, 2021